j mater res technol. 2018;xxx(xx):xxx–xxx

Available online at www.sciencedirect.com

jmr&t Journal of Materials Research and Technology

www.jmrt.com.br

Original Article

Phase prediction, microstructure and high hardness of novel light-weight high entropy alloys

Jon Mikel Sanchez[a], Iban Vicario[a], Joseba Albizuri[b], Teresa Guraya[c], Jose Carlos Garcia[a]

[a] Department of Foundry and Steel making, Tecnalia Research & Innovation, Derio, Spain
[b] Department of Mechanical Engineering, Faculty of Engineering of Bilbao (UPV/EHU), Bilbao, Spain
[c] Department of Mining & Metallurgical Engineering and Materials Science, Faculty of Engineering of Bilbao (UPV/EHU), Bilbao, Spain

ARTICLE INFO

Article history:
Received 21 April 2018
Accepted 13 June 2018
Available online xxx

Keywords:
High entropy alloys
High hardness
Light-weight
Calphad
Microstructure
Phase composition
Complex Concentrated Alloys

ABSTRACT

Guided by CALPHAD modeling, low-density and multiphase three novel High Entropy Alloys (HEAs), $Al_{40}Cu_{15}Cr_{15}Fe_{15}Si_{15}$, $Al_{65}Cu_5Cr_5Si_{15}Mn_5Ti_5$ and $Al_{60}Cu_{10}Fe_{10}Cr_5Mn_5Ni_5Mg_5$ were produced by large scale vacuum die casting. A mixture of simple and complex phases was observed in the as-cast microstructures, which demonstrates good agreement with CALPHAD results. The measured densities varied from 3.7 g/cm^3 to 4.6 g/cm^3 and microhardness from 743 Hv to 916 Hv. Finally, the hardness of all the light-weight HEAs (LWHEAs) with densities below 4.6 g/cm^3 manufactured to date were reviewed. The hardness of $Al_{40}Cu_{15}Cr_{15}Fe_{15}Si_{15}$ and hardness to density ratio of $Al_{65}Cu_5Cr_5Si_{15}Mn_5Ti_5$ are the highest of all LWHEAs reported up to date.

1. Introduction

HEAs have become a new research focus in the materials community in the last 14 years. The number of publications on this topic has grown enormously since the first publications in 2004 [1,2]. HEAs contains several major elements without a clear base element in contrast to conventional metallic alloys. The idea behind this new concept is that it is possible to stabilize a single phase solid solution (SS) by reducing Gibbs free energy, avoiding the formation of fragile intermetallic compounds (IC). Thus, the alloys are composed of five or more metallic elements in equimolar or nearly equimolar concentrations. HEAs have much higher mixing entropy values than traditional alloys in the liquid state or in the random SS state. Usually four "core effects" are used to describe the exceptional properties of HEAs: high entropy, sluggish diffusion, severe lattice distortion and cocktail effect [3]. Recently, a certain attention has been shifted to the study of multiphase HEAs with non-equiatomic compositions due to their excellent properties [4–11]. Multiphase HEAs are mainly composed of two phases, which are known as Complex Concentrated Alloys (CCAs). The term HEAs remained for the sake of simplicity and will be used throughout the present work. The vast range of complex compositions, microstructures and the properties of these novel alloys were reviewed by Miracle et al. [12] and Zhang et al. [13].

Considering that the total number of possible HEAs is around 10^{177} [14], the implementation of an efficient method for predicting phase formation in HEAs is critical

* Corresponding author.
E-mail: jonmikel.sanchez@tecnalia.com (J.M. Sanchez).
https://doi.org/10.1016/j.jmrt.2018.06.010

Please cite this article in press as: Sanchez JM, et al. Phase prediction, microstructure and high hardness of novel light-weight high entropy alloys. J Mater Res Technol. 2018. https://doi.org/10.1016/j.jmrt.2018.06.010

for the development of new engineering materials. Three types of methodologies have been developed for predicting phase formation in HEAs. At the beginning, various empirical thermo-physical parameters were proposed following the Hume–Rothery rules [15–18]. Gao et al. reviewed these parameters concluding that they are efficient in separating single-phase SS from amorphous alloys, but they fail to separate single-phase SS from multiphase microstructures [19]. More recently, the first-principles density functional theory (DFT) calculations combined with hybrid Monte Carlo/Molecular Dynamics (MC/MD) simulations have been applied to HEAs with reasonably success [20,21]. To date, the CALPHAD method can be regarded as the most robust method for HEAs design [22]. This method can accelerate the development of new HEAs through phase diagrams and phase stabilities calculated from multicomponent thermodynamic databases [23]. Most thermodynamic databases have been developed for specific commercial alloys, which mean that they usually have optimal compositional ranges of application. But HEAs are not based on a main element like traditional alloys. Therefore, some specific databases were developed for phase prediction in HEAs. This databases are TCHEA [24,25] and PanHEA [19,26] supplied by Thermo-Calc™ and Pandat™ respectively, but they are mainly restricted to transition metals containing HEAs. Thus, the latest version of TCHEA has been developed in a 26 element framework assessed to their full range of composition [27]. On the other hand, PanHEA database is actually restricted to 10 elements [28]. In some cases, the use of standard databases for commercial alloys such as TCAL and TCNI has shown acceptable efficacy in predicting phase stability of HEAs [29,30].

LWHEAs have recently attracted more attention for their excellent mechanical properties [31–35] and the possibility of reducing the weight in the transport or energy industry. In this work, only HEAs with a density equal to or less than commercial Ti alloys were defined as LWHEAs. Ti alloys are the heaviest of the light alloys used in engineering to reduce the weight of structures and components [36]. The pioneering LWHEA was nanocrystalline $Al_{20}Li_{20}Mg_{10}Sc_{20}Ti_{30}$ alloy, high hardness (591Hv) and low density (2.7 g/cm^3) were reported by Youssef et al. [37]. To date, the hardness and hardness to density ratio of $Al_{20}Be_{20}Fe_{10}Si_{15}Ti_{35}$ alloy are the highest reported before [38]. The estimated strength of this alloy is 2976 MPa, which is superior to those of traditional light-weight structural materials. Therefore, LWHEAs can be used as protective coating of machine components and tools because of their high hardness and excellent wear resistance [39].

Motivated by the above concerns, low-density and affordable $Al_{40}Cu_{15}Cr_{15}Fe_{15}Si_{15}$, $Al_{65}Cu_5Cr_5Si_{15}Mn_5Ti_5$ and $Al_{60}Cu_{10}Fe_{10}Cr_5Mn_5Ni_5Mg_5$ alloys were designed by CALPHAD method with the objective of achieving multiphase microstructure to exceed the hardness, wear behavior, and the performance of low-density alloys in high-temperature applications. The major driver of the alloy design was to reduce the density through increasing the molar % of Al, obtaining Al-based non-equimolar HEAs. This has allowed the good liquidity and castability of the molten alloys. Furthermore, the addition of Cr was critically necessary for the formation of high-temperature phases, while additions of Mn, Ni, Cu, Si and Fe enhanced solid solution strengthening. To reduce the alloy cost, expensive or scarce elements were avoided.

2. Experimental procedures

Thermo-Calc software (v. 2017b, Thermo-Calc Software AB, Stockholm, Sweden) [40] in conjunction with thermodynamic database TCAL5 was used for the equilibrium phases as a function of temperature calculation.

The raw elements with a minimum purity of 99.5 wt. % were melted and merged in an alumina crucible in an electric vacuum induction furnace model VIM (CONSARC, Rancocas, USA). Due to the high melting point of chromium, tablets of Al-Cr containing 75 wt. % of Cr were used. Before melting, a minimum chamber vacuum of 0.071 mbar was achieved and a protective Ar gas atmosphere was introduced to prevent oxidation reactions during melting, with a chamber pressure of 400 mbar. The molten alloy was poured and solidified into a metal die inside the furnace for at least 4 h.

Specimens of approximately 80 mm (length) × 80 mm (width) × 140 mm (thickness) were obtained from the as-cast material. The samples of each alloy were cut from the ingots and prepared according to standard metallographic procedures by hot mounting in conductive resin, grinding, and polishing.

The X-ray diffraction (XRD) equipment used to characterize the crystal structures of the alloys was a model D8 ADVANCE (BRUKER, Karlsruhe, Germany), with Cu Kα radiation, operated at 40 kV and 30 mA. The diffraction diagrams were measured at the diffraction angle 2θ, range from 10° to 90° with a step size of 0.01°, and 1.8 s/step. The powder diffraction file (PDF) database 2008 was applied for phase identification.

The microstructure, the different regions and the averaged overall chemical composition of each sample were investigated using a scanning electron microscope (SEM), equipped with an energy dispersive X-ray spectrometry (EDS) model JSM-5910LV (JEOL, Croissy-sur-Seine, France).

Vickers microhardness FM-700 model (FUTURE-TECH, Kawasaki, Japan) was performed on the polished sample surface using a 0.1 kg load, applied for 10 s. At least 10 random individual measurements were made. Finally, density measurement was conducted using the Archimedes method.

3. Results and discussion

The thermodynamic calculations of equilibrium phases in manufactured alloys as a function of temperature were calculated using Thermo-Calc software and TCAL5 database as shown in Fig. 1. TCAL5 database is commonly used for Al commercial alloys. But according to previous works [30,31], the use of this database in Al-based HEAs shows good agreement with the experimental results. Regarding the very low cooling rate used in the present study, it is reasonable to assume that the alloys are close to thermodynamic equilibrium. Nevertheless, it should be noted that calculations were made for homogeneous alloys and not considering impurities from the Al-Cr tablets or oxides formed during the casting process.

Please cite this article in press as: Sanchez JM, et al. Phase prediction, microstructure and high hardness of novel light-weight high entropy alloys. J Mater Res Technol. 2018. https://doi.org/10.1016/j.jmrt.2018.06.010

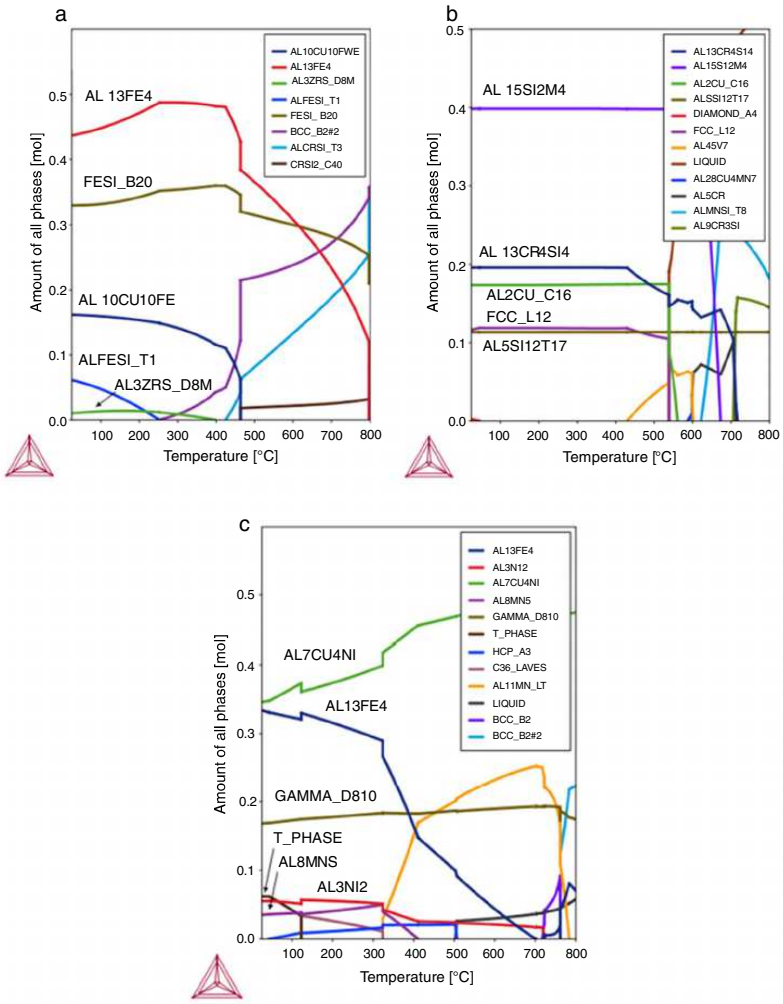

Fig. 1 – Calculated phase diagrams of the manufactured alloys (a) $Al_{40}Cu_{15}Cr_{15}Fe_{15}Si_{15}$, (b) $Al_{65}Cu_5Cr_5Si_{15}Mn_5Ti_5$ and (c) $Al_{60}Cu_{10}Fe_{10}Cr_5Mn_5Ni_5Mg_5$; using Thermo-Calc software with TCAL5 database.

Fig. 1(a) shows that no major change is expected below 246 °C in $Al_{40}Cu_{15}Cr_{15}Fe_{15}Si_{15}$ cast alloy, which is the temperature of precipitation of the AlFeSi (τ_1) phase. The τ_1 phase is predicted to slightly grow at the expense of BCC (B2) phase. The simulation suggested the formation of five phases at room temperature (RT), but the amount of Al_3Zr_5 (D8m) is insignificant. The solidus temperature is 800 °C. In Fig. 1(b), five phases were predicted in equilibrium at RT for $Al_{65}Cu_5Cr_5Si_{15}Mn_5Ti_5$ cast alloy. All the phases are stable below 429 °C, and the solidus temperature is 534 °C. According to the Thermo-Calc equilibrium phase diagram of $Al_{60}Cu_{10}Fe_{10}Cr_5Mn_5Ni_5Mg_5$ cast alloy in Fig. 1(c), some qualitative and quantitative changes are expected below 326 °C in Al_8Mn_5 and τ_1-AlFeSi phase. The solidus temperature is 506 °C. The whole quantity of these minor phases only represents 10 mol % of the amount of phase at RT. The diagrams suggest high phase stability of the designed alloys at high temperatures.

In Table 1, the thermodynamic calculations of equilibrium phases were summarized with the detailed description of their phase constitution and the amount of phase. The phase constitution obtained by TCAL5 database reflects that multiple elements can be dissolved in the sublattices. The amount of each element calculated for each sublattice has been neglected, this analysis has only been considered in a qualitative and not a quantitative way. Although the alloys are close to thermodynamic equilibrium, they are not expected to be in complete equilibrium. In addition, is supposed that the above mentioned high entropy, sluggish diffusion and severe lattice distortion effects can enrich the solution of the elements in each phase.

Please cite this article in press as: Sanchez JM, et al. Phase prediction, microstructure and high hardness of novel light-weight high entropy alloys. J Mater Res Technol. 2018. https://doi.org/10.1016/j.jmrt.2018.06.010

Table 1 – Phases predicted, phase constitution and amount of phase (mol %) of $Al_{40}Cu_{15}Fe_{10}Cr_{15}Fe_{15}Si_{15}$ (HEA1), $Al_{65}Cu_5Cr_5Si_{15}Mn_5Ti_5$ (HEA2) and $Al_{60}Cu_{10}Fe_{10}Cr_5Mn_5Ni_5Mg_5$ (HEA3) cast alloys, using of Thermo-Calc software with TCAL5 database.

Alloy	Phase	Phase constitution	Mol %
HEA1	$Al_{10}Cu_{10}Fe$	$(Fe)_1$ $(Al,Cu)_{10}$ $(Al)_{10}$	16
	$Al_{13}Fe_4$	$(Al,Cu)_{0.63}$ $(Fe)_{0.23}$ $(Al,Si,VA)_{0.14}$	43
	Al_3Zr_5 (D8m)	$(Al,Si)_3$ $(Cr)_5$	1
	AlFeSi (τ_1)	$(Al,Si)_5$ $(Fe)_3$	7
	FeSi (B20)	$(Cr,Fe)_1$ $(Al,Si)_1$	33
HEA2	$Al_{13}Cr_4Si_4$	$(Al)_{13}$ $(Cr)_4$ $(Si)_4$	20
	$Al_{15}Si_2Mn_4$	$(Al)_{16}$ $(Mn)_4$ $(Si)_1$ $(Al,Si)_2$	40
	Al_2Cu (C16)	$(Al,Mn)_2$ $(Al,Cu,Mn,Si)_1$	18
	$Al_5Si_{12}Ti_7$	$(Al,Si)_{0.21}$ $(Si)_{0.5}$ $(Ti)_{0.29}$	11
	FCC ($L1_2$)	$(Al,Cr,Cu,Mn,Si,Ti)_{0.75}(Al,Cr,Cu,Mn,Si,Ti)_{0.25}$ $(VA)_1$	11
HEA3	$Al_{13}Fe_4$	$(Al,Cu)_{0.63}$ $(Fe,Mn,Ni)_{0.23}$ $(Al,VA)_{0.14}$	33
	Al_3Ni_2	$(Al)_3$ $(Al,Cu,Fe,Mg,Ni)_2$ $(Ni,VA)_1$	6
	Al_7Cu_4Ni	$(Al)_1$ $(Cu,Fe,Ni,VA)_1$	35
	Al_8Mn_5	$(Al)_{12}$ $(Mn)_5$ $(Al,Cu,Mn)_9$	4
	Υ ($D8_{10}$)	$(Al)_{12}$ $(Cr)_5$ $(Al,Cr)_9$	16
	τ-phase	$(Mg)_{26}$ $(Al,Mg)_6$ $(Al,Cu,Mg)_{48}$ $(Al)_1$	6

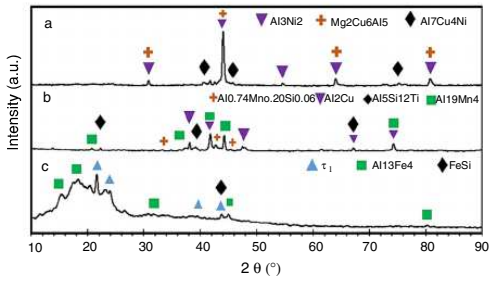

Fig. 2 – XRD diffraction patterns of the cast (a) $Al_{40}Cu_{15}Fe_{10}Cr_{15}Fe_{15}Si_{15}$, (b) $Al_{65}Cu_5Cr_5Si_{15}Mn_5Ti_5$ and (c) $Al_{60}Cu_{10}Fe_{10}Cr_5Mn_5Ni_5Mg_5$.

According to Thermo-Calc simulations, a multiphase character can be expected for the manufactured alloys, which is proven by the results of XRD measurements shown in Fig. 2. Considering that the intensities of the diffraction peaks of ordered phases are stronger than those of SS phases, the volume fractions of non-stoichiometric compounds appear to predominate.

Fig. 2(a) shows the XRD patterns of the as-cast $Al_{40}Cu_{15}Cr_{15}Fe_{15}Si_{15}$ alloy. The XRD peaks of the alloy corresponds to $Al_{13}Fe_4$, $Fe_3Al_2Si_3$ (τ_1) and FeSi phases. All phases present low diffraction peaks, except $Al_{13}Fe_4$ phase at 22° and 24°. Thus, all the phases predicted by Thermo-Calc were observed in XRD diagram, with the exception of $Al_{10}Cu_{10}Fe$ andAl_3Zr_5 (D8m) phase. Fig. 2(b) shows the XRD pattern of the as-cast $Al_{65}Cu_5Cr_5Si_{15}Mn_5Ti_5$ alloy. All the phases in equilibrium predicted by Thermo-Calc were observed, except $Al_{13}Cr_4Si_4$ phase. These phases were indexed as $Al_{13}Cr_4Si_4$, $Al_{0.74}Mn_{0.20}Si_{0.06}$, Al_2Cu, $Al_5Si_{12}Ti_7$ and $Al_{19}Mn_4$. FCC ($L1_2$) and $Al_{15}Si_2Mn_4$ phases predicted by Thermo-Calc corresponds to $Al_{19}Mn_4$ and $Al_{0.74}Mn_{0.20}Si_{0.06}$ respectively. The corresponding XRD pattern of the as-cast $Al_{60}Cu_{10}Fe_{10}Cr_5Mn_5Ni_5Mg_5$ alloy is shown in Fig. 2(c). Strong diffraction peak is observed at 44°, corresponding to Al_3Ni_2 and Al_7Cu_4Ni phases. The last phase was indexed as cubic $Mg_2Cu_6Al_5$ phase, which was correlated to $Mg_2Cu_6Al_5$. The volume fractions of constitutive phases were calculated experimentally by XRD and detailed in Table 2. In HEA1, the experimental volume fraction of the phases is consistent with thermodynamic calculations of FeSi and τ_1-AlFeSi phases in Table 1. But the phase volume of $Al_{13}Fe_4$ calculated by XRD is quite higher. In HEA2, the predicted volume of phase and the experimental result obtained by XRD are in good accordance. In HEA3, fewer phases than those calculated by Thermo-Calc were observed in the XRD patterns. Thus, the volume fractions are slightly different. Experimental data suggest that Al_3Ni_2 is the main phase in the microstructure, in contrast to the amount of phase obtained by Thermo-Calc in Table 1. The major crystallographic data is summarized in Table 2.

The overall bulk composition of the alloys was estimated using EDS on large areas. At least three random measurements were made and the overall values are presented in Table 3. Overall values of $Al_{60}Cu_{10}Fe_{10}Cr_5Mn_5Ni_5Mg_5$ alloy, slightly deviate from the nominal concentration due evaporation losses of Mg during the melting process.

Fig. 3(a) shows the SEM micrograph of the polished surface of as-cast $Al_{40}Cu_{15}Cr_{15}Fe_{15}Si_{15}$ alloy. In Fig. 3(b) the marked surface was magnified to identify small region marked as oxides, this region cannot be observed in Fig. 3(a) due to the negligible amount of phase that it represents in the alloy. The main areas in the morphology of the alloy are Region 1 and Region 2 (dark compounds). Surrounded by these regions, it can be observed Region 3 and a small amount of oxides.

In Fig. 4(a) qualitative elemental mapping was conducted by EDS to identify the distribution of elements in the observed regions. The results agree well with Fig. 3 and three areas can be distinguished in the elemental mapping. The main areas in the morphology of the alloy are Region 1, which is rich in Al-Cr and Region 2, rich in Al-Fe. Surrounded by these regions, it can be observed (Al,Cu)-rich area (Region 3) and small amount of oxides. From the EDS pattern in Fig. 4(b), it can be observed

Please cite this article in press as: Sanchez JM, et al. Phase prediction, microstructure and high hardness of novel light-weight high entropy alloys. J Mater Res Technol. 2018. https://doi.org/10.1016/j.jmrt.2018.06.010

Table 2 – List of phases, volume fraction (mol %), Space Group and the lattice parameters of $Al_{40}Cu_{15}Fe_{10}Cr_{15}Fe_{15}Si_{15}$ (HEA1), $Al_{65}Cu_5Cr_5Si_{15}Mn_5Ti_5$ (HEA2) and $Al_{60}Cu_{10}Fe_{10}Cr_5Mn_5Ni_5Mg_5$ (HEA3) cast alloys obtained by XRD.

Alloy	Phase	Space Group	Volume fraction	Lattice parameter (Å)
HEA1	$Al_{13}Fe_4$	B2/m (10)	57	$a = 15.49$, $b = 8.08$, $c = 12.48$
	τ_1-AlFeSi	P1 (2)	10	$a = 4.65$, $b = 3.27$, $c = 7.50$
	FeSi	P213 (198)	33	$a = b = c = 4.49$
HEA2	$Al_{0.74}Mn_{0.20}Si_{0.06}$	Pm3 (200)	47	$a = b = c = 9.71$
	Al_2Cu	I4/mcm (140)	2	$a = b = 6.07$, $c = 4.89$
	$Al_5Si_{12}Ti_7$	$I4_1$/amd (141)	13	$a = b = 3.57$, $c = 27.15$
	$Al_{19}Mn_4$	Pm3 (200)	13	$a = b = c = 12.68$
HEA3	Al_3Ni_2	P3m1 (164)	77	$a = b = 4.22$, $c = 5.16$
	Al_7Cu_4Ni	R3m (166)	7	$a = b = 4.10$, $c = 39.97$
	$Mg_2Cu_6Al_5$	Pm3 (200)	15	$a = b = c = 8.31$

Table 3 – Chemical composition in at. % of the manufactured alloys.

Alloy	Al	Cu	Fe	Cr	Si	Mn	Ti	Ni	Mg
$Al_{40}Cu_{15}Cr_{15}Fe_{15}Si_{15}$	41	13	14	16	16	–	–	–	–
$Al_{65}Cu_5Cr_5Si_{15}Mn_5Ti_5$	66	6	–	4	13	7	4	–	–
$Al_{60}Cu_{10}Fe_{10}Cr_5Mn_5Ni_5Mg_5$	60	11	10	6	–	5	–	6	2

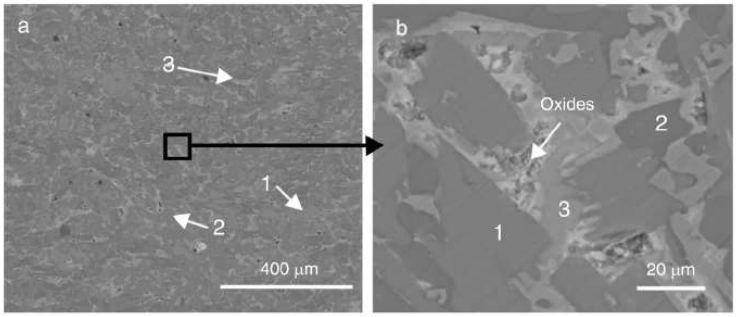

Fig. 3 – (a) SEM image of cast $Al_{40}Cu_{15}Cr_{15}Fe_{15}Si_{15}$ alloy (b) high magnification of marked surface.

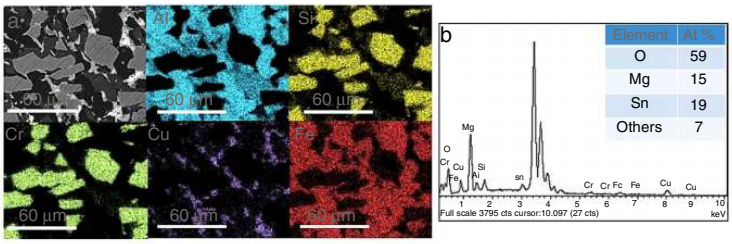

Fig. 4 – (a) EDS elemental mapping of cast $Al_{40}Cu_{15}Cr_{15}Fe_{15}Si_{15}$ alloy and (b) EDS pattern of oxides-region.

that the oxides region is mainly composed of impurities such as O, Mg and Sn.

Fig. 5(a) shows the complex morphology of $Al_{65}Cu_5Cr_5Si_{15}Mn_5Ti_5$ alloy, the microstructure is composed of four different regions. The contrast between regions is relatively high due to their complex compositions, which are composed of at least three elements. In Fig. 5(b), the marked surface was magnified for a better understanding of the complex morphology of the alloy.

Elemental mapping was conducted by EDS as shown in Fig. 6 to identify the distribution of elements in the observed regions. The microstructure shows a matrix composed of Al-rich area (Region 1) and Al-Cu-rich area (Region 2). The brightest region is marked as Region 3, this region is composed

Please cite this article in press as: Sanchez JM, et al. Phase prediction, microstructure and high hardness of novel light-weight high entropy alloys. J Mater Res Technol. 2018. https://doi.org/10.1016/j.jmrt.2018.06.010

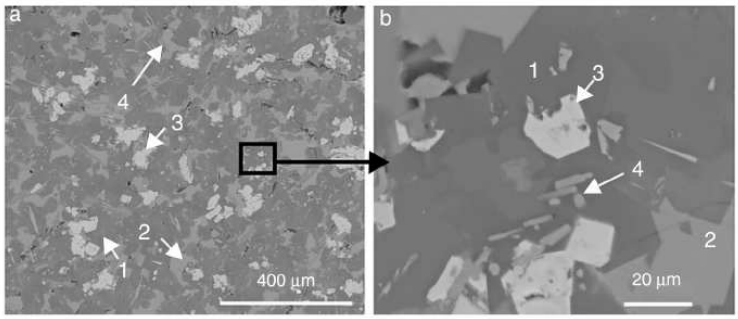

Fig. 5 – (a) SEM image of cast $Al_{65}Cu_5Cr_5Si_{15}Mn_5Ti_5$ alloy (b) high magnification of marked surface.

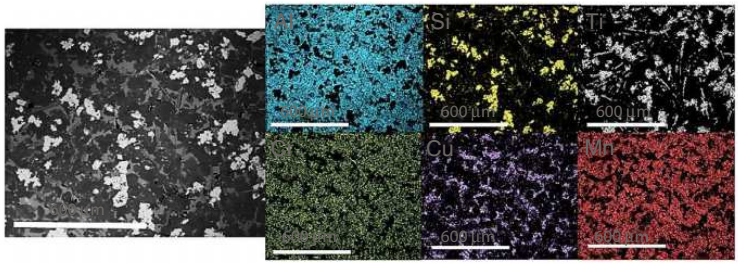

Fig. 6 – EDS elemental mapping of cast $Al_{65}Cu_5Cr_5Si_{15}Mn_5Ti_5$ alloy.

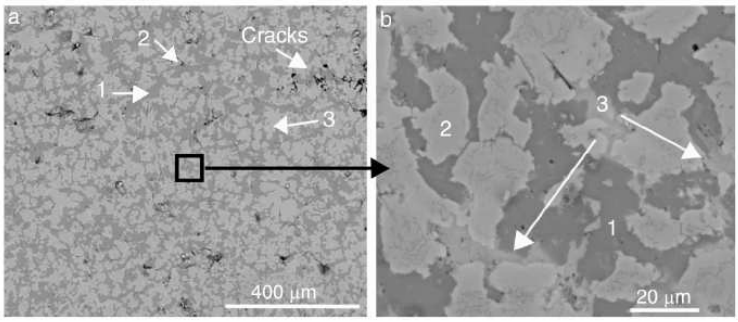

Fig. 7 – (a) SEM image of cast $Al_{60}Cu_{10}Fe_{10}Cr_5Mn_5Ni_5Mg_5$ alloy (b) high magnification of marked surface.

of Si and Ti. Finally, needle-like and irregularly sized Region 4 can be observed not homogeneously distributed throughout the whole alloy.

The SEM image in Fig. 7 of $Al_{60}Cu_{10}Fe_{10}Cr_5Mn_5Ni_5Mg_5$ alloy shows a typical dendritic microstructure, indicating constitutional segregation during the non-equilibrium solidification. In contrast to Thermo-Calc predictions but accordingly with XRD results, only three regions can be distinguished. Fine cracks are also observed in Fig. 7(a).

In Fig. 8 Elemental mapping was conducted by EDS to identify the distribution of elements in the observed regions. The dendrites (Region 1) as well as the interdendritic area (Region 2) consist of a mixture of all the elements in the alloy except Mg. The amount of Ni in the interdendritic region is significantly higher than in the dendritic region. There is compositional segregation inside the interdendritic region of Mg and Cu, marked as Region 3. As can be seen in Fig. 7(a), the main region of the alloy is Region 2. From elemental composition obtained in Fig. 8 and the phase constitution predicted in Table 1, Al_3Ni_2 phase (Table 2) was correlated to the dendritic region. Moreover, this shows good agreement with the volumetric fraction of phases obtained experimentally in Table 2.

The microhardness of the fabricated alloys was evaluated on Vickers microhardness tester. The mean microhardness values with the standard deviation are 916 ± 99 Hv for $Al_{40}Cu_{15}Cr_{15}Fe_{15}Si_{15}$, 889 ± 281 Hv for $Al_{65}Cu_5Cr_5Si_{15}Mn_5Ti_5$ and 743 ± 95 for $Al_{60}Cu_{10}Fe_{10}Cr_5Mn_5Ni_5Mg_5$ alloy. The standard deviation of the microhardness in $Al_{65}Cu_5Cr_5Si_5Mn_5Ti_5$ is very large due to the complex morphology observed in Fig. 5. Table 4 lists the microhardness and density of manufactured

Please cite this article in press as: Sanchez JM, et al. Phase prediction, microstructure and high hardness of novel light-weight high entropy alloys. J Mater Res Technol. 2018. https://doi.org/10.1016/j.jmrt.2018.06.010

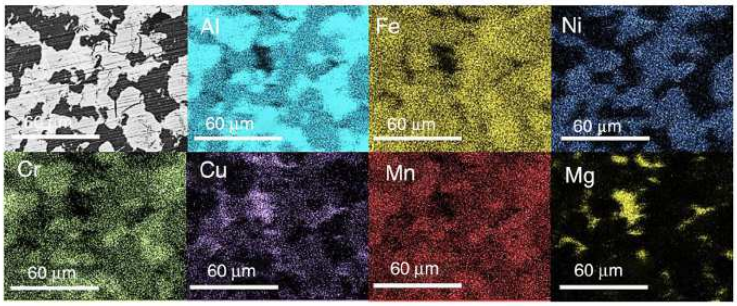

Fig. 8 – EDS elemental mapping of as-cast $Al_{60}Cu_{10}Fe_{10}Cr_5Mn_5Ni_5Mg_5$ alloy.

Table 4 – Density and microhardness of manufactured alloys in comparison with other published results.

Alloy	ρ (g.cm^{-3})	Hardness (Hv)	Ref.
$Al_{40}Cu_{15}Cr_{15}Fe_{15}Si_{15}$	4.5	916	–
$Al_{65}Cu_5Cr_5Si_{15}Mn_5Ti_5$	3.7	889	–
$Al_{60}Cu_{10}Fe_{10}Cr_5Mn_5Ni_5Mg_5$	4.6	743	–
$Al_{20}Li_{20}Mg_{10}Sc_{20}Ti_{30}$	2.7	591	[37]
$Al_{20}Be_{20}Fe_{10}Si_{15}Ti_{35}$	3.9	911	[38]
$Mg_{20}(MnAlZnCu)_{80}$	4.3	431	[33]
$Mg_{33}(MnAlZnCu)_{77}$	3.3	310	[33]
$Mg_{43}(MnAlZnCu)_{67}$	2.5	250	[33]
$Mg_{45.6}(MnAlZnCu)_{54.4}$	2.4	225	[33]
$Mg_{50}(MnAlZnCu)_{50}$	2.2	178	[33]
MgMnAlZnCu (air cooling)	4.3	431	[34]
MgMnAlZnCu (water cooling)	4.3	449	[34]
MgMnAlZnCu (salt water cooling)	4.3	467	[34]
$Al_{40}Cu_{15}Mn_5Ni_5Si_{20}Zn_{15}$	4.1	887	[31]
$Al_{35}Cu_5Fe_5Mn_5Si_{30}V_{10}Zr_{10}$	4.0	751	[31]
$Al_{50}Ca_5Cu_5Ni_{10}Si_{20}Ti_{10}$	3.3	437	[31]

alloys in present work, and previously reported LWHEAs with density below 4.6 g/cm^3.

To date, the hardness of $Al_{40}Cu_{15}Cr_{15}Fe_{15}Si_{15}$ alloy is the highest value reported for a LWHEA. In addition, the hardness to density ratio of $Al_{65}Cu_5Cr_5Si_{15}Mn_5Ti_5$ is the highest reported to date. $Al_{40}Cu_{15}Cr_{15}Fe_{15}Si_{15}$ and $Al_{60}Cu_{10}Fe_{10}Cr_5Mn_5Ni_5Mg_5$ alloys have similar density to pure Ti and Ti-6Al-4V alloys, for which the common hardness values range is from 200 to 369 Hv [41]. But the hardness of $Al_{40}Cu_{15}Cr_{15}Fe_{15}Si_{15}$ and $Al_{60}Cu_{10}Fe_{10}Cr_5Mn_5Ni_5Mg_5$ is considerably higher. According to the Tabor relation [42], the Vickers hardness divided by 3 should approximate the yield strength. Values estimated by this way are 2994 MPa for $Al_{40}Cu_{15}Cr_{15}Fe_{15}Si_{15}$, 2916 MPa for $Al_{65}Cu_5Cr_5Si_{15}Mn_5Ti_5$ and 2429 MPa for $Al_{60}Cu_{10}Fe_{10}Cr_5Mn_5Ni_5Mg_5$ alloy. These values are higher than tungsten high speed tool steels and to those of traditional structural materials.

4. Conclusions

In summary, three novel $Al_{40}Cu_{15}Cr_{15}Fe_{15}Si_{15}$, $Al_{65}Cu_5Cr_5Si_{15}Mn_5Ti_5$ and $Al_{60}Cu_{10}Fe_{10}Cr_5Mn_5Ni_5Mg_5$ LWHEAs were designed by Thermo-Calc in conjunction with TCAL5 database and produced by large scale vacuum die casting. In addition, low density and high hardness from 743 to 916 Hv was reported for manufactured alloys.

The LWHEAs have been fabricated by large-scale vacuum die casting. Our results suggested that affordable LWHEAs with high hardness can be adapted to large-scale industrial production.

There are some discrepancies between the experimental results and Thermo-Calc calculations. CALPHAD thermodynamic modeling successfully predicted the constituent phases, which are consistent with the experimental results. However, more phases are predicted by Thermo-Calc in $Al_{40}Cu_{15}Cr_{15}Fe_{15}Si_{15}$ and $Al_{60}Cu_{10}Fe_{10}Cr_5Mn_5Ni_5$ alloys at RT than those observed in the samples. This suggests that despite having a slow cooling rate of solidification, total equilibrium state is not achieved in the manufacturing of the alloys. In general, this database has proven to be a good method for designing Al-based HEAs.

The high microhardness of the manufactured alloys is due to the presence of complex precipitates containing multiple elements on their respective sublattices as strengtheners.

New LWHEAs can provide a combination of low density and microstructures that could increase wear, strength, and performance at high temperatures of traditional light-weight alloys. The hardness of $Al_{40}Cu_{15}Cr_{15}Fe_{15}Si_{15}$ and hardness to density ratio of $Al_{65}Cu_5Cr_5Si_{15}Mn_5Ti_5$ are the highest of all LWHEAs previously reported. Therefore, we estimate

Please cite this article in press as: Sanchez JM, et al. Phase prediction, microstructure and high hardness of novel light-weight high entropy alloys. J Mater Res Technol. 2018. https://doi.org/10.1016/j.jmrt.2018.06.010

that these newly designed LWHEAs have wide application prospects and can be of interest for future research. In addition to the applications mentioned above, we propose these alloys to be used as casing or structural materials of laptops or smartphones. For this, low density materials with high strength and especially high hardness are required to avoid scratches and protect the electronics.

Conflicts of interest

The authors declare no conflict of interest.

Acknowledgments

This work has been partially funded by the Basque government through the project Elkartek: KK-2017/00007.

REFERENCES

[1] Yeh JW, Chen SK, Lin SJ, Gan JY, Chin TS, Shun TT, et al. Nanostructured high-entropy alloys with multiple principal elements: novel alloy design concepts and outcomes. Adv Eng Mater 2004;6:299–303, http://dx.doi.org/10.1002/adem.200300567, 274.
[2] Cantor B, Chang ITH, Knight P, Vincent AJB. Microstructural development in equiatomic multicomponent alloys. Mater Sci Eng A 2004;375–377:213–8, http://dx.doi.org/10.1016/j.msea.2003.10.257.
[3] Zhang Y, Zuo TT, Tang Z, Gao MC, Dahmen KA, Liaw PK, et al. Microstructures and properties of high-entropy alloys. Prog Mater Sci 2014, http://dx.doi.org/10.1016/j.pmatsci.2013.10.001.
[4] Alaneme KK, Bodunrin MO, Oke SR. Processing, alloy composition and phase transition effect on the mechanical and corrosion properties of high entropy alloys: a review. J Mater Res Technol 2015;5:384–93, http://dx.doi.org/10.1016/j.jmrt.2016.03.004.
[5] Zhou Y, Zhou D, Jin X, Zhang L, Du X, Li B. Design of non-equiatomic medium-entropy alloys. Sci Rep 2018;8, http://dx.doi.org/10.1038/s41598-018-19449-0, 1DUMMY.
[6] Raabe D, Tasan CC, Springer H, Bausch M. From high-entropy alloys to high-entropy steels. Steel Res Int 2015;86:1127–38, http://dx.doi.org/10.1002/srin.201500133.
[7] Zhang H, Tang H, Li WH, Wu JL, Zhong XC, Chen G, et al. Novel high-entropy and medium-entropy stainless steels with enhanced mechanical and anti-corrosion properties. Mater Sci Technol (United Kingdom) 2017:1–8, http://dx.doi.org/10.1080/02670836.2017.1416907.
[8] Pradeep KG, Tasan CC, Yao MJ, Deng Y, Springer H, Raabe D. Non-equiatomic high entropy alloys: approach towards rapid alloy screening and property-oriented design. Mater Sci Eng A 2015;648:183–92, http://dx.doi.org/10.1016/j.msea.2015.09.010.
[9] Stepanov ND, Shaysultanov DG, Tikhonovsky MA, Salishchev GA. Tensile properties of the Cr-Fe-Ni-Mn non-equiatomic multicomponent alloys with different Cr contents. Mater Des 2015;87:60–5, http://dx.doi.org/10.1016/j.matdes.2015.08.007.
[10] Li Z, Pradeep KG, Deng Y, Raabe D, Tasan CC. Metastable high-entropy dual-phase alloys overcome the strength-ductility trade-off. Nature 2016;534:227–30, http://dx.doi.org/10.1038/nature17981.
[11] Gorsse S, Miracle DB, Senkov ON. Mapping the world of complex concentrated alloys. Acta Mater 2017;135:177–87, http://dx.doi.org/10.1016/j.actamat.2017.06.027.
[12] Miracle DB, Senkov ON. A critical review of high entropy alloys and related concepts. Acta Mater 2017, http://dx.doi.org/10.1016/j.actamat.2016.08.081.
[13] Zhang W, Liaw PK, Zhang Y. Science and technology in high-entropy alloys. Sci China Mater 2018;61:2–22, http://dx.doi.org/10.1007/s40843-017-9195-8.
[14] Cantor B. Multicomponent and high entropy alloys. Entropy 2014;16:4749–68, http://dx.doi.org/10.3390/e16094749.
[15] Yang X, Zhang Y. Prediction of high-entropy stabilized solid-solution in multi-component alloys. Mater Chem Phys 2012;132:233–8, http://dx.doi.org/10.1016/j.matchemphys.2011.11.021.
[16] Zhang Y, Zhou YJ, Lin JP, Chen GL, Liaw PK. Solid-solution phase formation rules for multi-component alloys. Adv Eng Mater 2008;10:534–8, http://dx.doi.org/10.1002/adem.200700240.
[17] Guo S. Phase selection rules for cast high entropy alloys: an overview. Mater Sci Technol 2015;31:1223–30, http://dx.doi.org/10.1179/1743284715Y. 0000000018.
[18] Guo S, Ng C, Lu J, Liu CT. Effect of valence electron concentration on stability of fcc or bcc phase in high entropy alloys. J Appl Phys 2011:109, http://dx.doi.org/10.1063/1.3587228.
[19] Gao MC, Zhang C, Gao P, Zhang F, Ouyang LZ, Widom M, et al. Thermodynamics of concentrated solid solution alloys. Curr Opin Solid State Mater Sci 2017;21:238–51, http://dx.doi.org/10.1016/j.cossms.2017.08.001.
[20] Tian F, Varga LK, Chen N, Delczeg L, Vitos L. Ab initio investigation of high-entropy alloys of 3d elements. Phys Rev B – Condens Matter Mater Phys 2013:87, http://dx.doi.org/10.1103/PhysRevB.87.075144.
[21] Liu Z, Lei Y, Gray C, Wang G. Examination of solid-solution phase formation rules for high entropy alloys from atomistic Monte Carlo simulations. JOM 2015;67:2364–74, http://dx.doi.org/10.1007/s11837-015-1508-3.
[22] Gao MC, Liaw PK, Yeh J-W, Zhang Y. High-entropy alloys: fundamentals and applications 2016, http://dx.doi.org/10.1007/978-3-319-27013-5.
[23] Zhang F, Zhang C, Chen SL, Zhu J, Cao WS, Kattner UR. An understanding of high entropy alloys from phase diagram calculations. Calphad Comput Coupling Phase Diagr Thermochem 2014;45:1–10, http://dx.doi.org/10.1016/j.calphad.2013.10.006.
[24] Chen HL, Mao H, Chen Q. Database development and Calphad calculations for high entropy alloys: challenges, strategies, and tips. Mater Chem Phys 2018;210:279–90, http://dx.doi.org/10.1016/j.matchemphys.2017.07.082.
[25] Mao H, Chen HL, Chen Q. TCHEA1: a thermodynamic database not limited for "High Entropy" alloys. J Phase Equilibria Diffus 2017;38:353–68, http://dx.doi.org/10.1007/s11669-017-0570-7.
[26] Zhang C, Zhang F, Diao H, Gao MC, Tang Z, Poplawsky JD, et al. Understanding phase stability of Al-Co-Cr-Fe-Ni high entropy alloys. Mater Des 2016;109:425–33, http://dx.doi.org/10.1016/j.matdes.2016.07.073.
[27] https://www.thermocalc.com/.
[28] https://www.computherm.com/.
[29] Feng R, Gao M, Lee C, Mathes M, Zuo T, Chen S, et al. Design of light-weight high-entropy alloys. Entropy 2016;18:333, http://dx.doi.org/10.3390/e18090333.
[30] Sun W, Huang X, Luo AA. Phase formations in low density high entropy alloys. Calphad Comput Coupling Phase Diagr Thermochem 2017;56:19–28, http://dx.doi.org/10.1016/j.calphad.2016.11.002.
[31] Sanchez JM, Vicario I, Albizuri J, Guraya T, Koval N, Garcia J. Compound formation and microstructure of As-cast high entropy aluminiums. Metals (Basel) 2018;8:167, http://dx.doi.org/10.3390/met8030167.

Please cite this article in press as: Sanchez JM, et al. Phase prediction, microstructure and high hardness of novel light-weight high entropy alloys. J Mater Res Technol. 2018. https://doi.org/10.1016/j.jmrt.2018.06.010

[32] Feng R, Gao MC, Zhang C, Guo W, Poplawsky JD, Zhang F, et al. Phase stability and transformation in a light-weight high-entropy alloy. Acta Mater 2018; 146:280–93, http://dx.doi.org/10.1016/j.actamat.2017.12.061.
[33] Li R, Gao J, Fa K. Study to microstructure and mechanical properties of Mg containing high entropy alloys. Mater Sci Forum 2010;650: 265–71, http://dx.doi.org/10.4028/www.scientific.net/MSF.650.265.
[34] Li R, Gao J-C, Fan K. Microstructure and mechanical properties of MgMnAlZnCu high entropy alloy cooling in three conditions. Mater Sci Forum 2011;686: 235–41, http://dx.doi.org/10.4028/www.scientific.net/MSF.686.235.
[35] Yang X, Chen SY, Cotton JD, Zhang Y. Phase stability of low-density, multiprincipal component alloys containing aluminium, magnesium, and lithium. JOM 2014; 66:2009–20, http://dx.doi.org/10.1007/s11837-014-1059-z.
[36] Polmear IP. Light alloys – from traditional alloys to nanocrystals, vol. 2; 2006, http://dx.doi.org/10.1017/CBO9781107415324.004.
[37] Youssef KM, Zaddach AJ, Niu C, Irving DL, Koch CC. A novel low-density, high-hardness, high-entropy alloy with close-packed single-phase nanocrystalline structures. Mater Res Lett 2014;3:95–9, http://dx.doi.org/10.1080/21663831.2014.985855.
[38] Tseng K, Yang Y, Juan C, Chin T, Tsai C, Yeh J. A light-weight high-entropy alloy Al20Be20Fe10Si15Ti35. Sci China Technol Sci 2017;841:18–23, http://dx.doi.org/10.1007/s11431-017-9073-0.
[39] Kumar A, Gupta M. An insight into evolution of light weight high entropy alloys: a review. Metals (Basel) 2016;6:199, http://dx.doi.org/10.3390/met6090199.
[40] Andersson JO, Helander T, Höglund L, Shi P, Sundman B. Thermo-Calc & DICTRA, computational tools for materials science. Calphad Comput Coupling Phase Diagr Thermochem 2002;26:273–312, http://dx.doi.org/10.1016/S0364-5916(02)00037-8.
[41] Da Rocha SS, Adabo GL, Henriques GEP, Nóbilo MADA. Vickers hardness of cast commercially pure titanium and Ti-6Al-4V alloy submitted to heat treatments. Braz Dent J 2006;17:126–9, http://dx.doi.org/10.1590/S0103-64402006000200008.
[42] Tabor D. The physical meaning of indentation and scratch hardness. Br J Appl Phys 1956;7:159–66, http://dx.doi.org/10.1088/0508-3443/7/5/301.

Please cite this article in press as: Sanchez JM, et al. Phase prediction, microstructure and high hardness of novel light-weight high entropy alloys. J Mater Res Technol. 2018. https://doi.org/10.1016/j.jmrt.2018.06.010